Numerical Simulations of Autoignition in Turbulent Mixing Flows

E. MASTORAKOS* AND T. A. BARITAUD

Centre de Recherche sur la Combustion Turbulente, Institut Français du Pétrole, 1 avenue de Bois-Preau, 92506 Rueil-Malmaison, France

T. J. POINSOT

IMFT / CERFACS, 42 ave G. Coriolis, 31057 Toulouse, France

Two-dimensional direct numerical simulations have been performed of the autoignition of (i) laminar and turbulent shearless mixing layers between fuel and hotter air, (ii) thin slabs of fuel exposed to air from both sides, and (iii) homogeneous stagnant adiabatic mixtures. It has been found that the time for the first appearance of an ignition site is almost independent of the turbulence time scale, varies little in individual realisations of the same flow, decreases with partial premixing, is shorter in turbulent than in laminar flows, and decreases with decreasing width of the fuel stream. The autoignition time in the turbulent flows is longer than the ignition delay time of stagnant homogeneous mixtures and this implies that the heat losses due to mixture fraction gradients associated with mixture inhomogeneities increase the autoignition time. It has also been found that ignition always occurs at a well-defined mixture fraction f_{MR}, which is accurately predicted by previous laminar flow analyses to depend only on the fuel and oxidant temperatures and the activation energy. As a measure of the heat losses of the heat-producing regions that eventually autoignite, the time evolution of the scalar dissipation rate, conditional on the most reactive mixture fraction, is examined and used to explain successfully all the observed trends of autoignition time with turbulent time scale, flow length scale, and partial premixing. The implications of these findings for modelling and for the interpretation of experimental data are discussed.

NOMENCLATURE

b	reactedness; Eq. 7
c_p	specific heat capacity
c_{ref}	sound velocity; Section 2
f	mixture fracture; Eq. 5
f_o	mixture fraction of fuel stream; Section 2.2
k	turbulent kinetic energy
L	length
L_{box}	length of calculation domain
L_f	estimate of the distance between f_{MR} and f_{st} fluid; Eq. 9
L_{ref}	reference length used for nondimensionalisation
L_{turb}	turbulent integral length scale; Section 2.2
P	pressure
Pr	Prandtl number
Q	heat release per unit mass of fuel
Re	Reynolds number, defined by $c_{ref} L_{ref}/\nu$
Re_t	turbulent Reynolds number, defined by $k^{1/2} L_{turb}/\nu$
S_{df}	average propagation speed of ignition fronts to f_{st}; Eq. 10
S_L	laminar burning velocity; Section 3.3
Sc	Schmidt number
t	time; Section 2.1
t_{ref}	reference time; Section 2.2 (equal to L_{ref}/c_{ref})
T	temperature
T_{in}	temperature of inert mixing used also as the initial condition; Eq. 3
T_{act}	activation temperature
w	width of fuel stream in slab calculations
W	reaction rate
x	coordinate
x_o	position of the centre of the initial fuel–air interface
y	coordinate
Y_1	local fuel mass fraction
Y_2	local oxygen mass fraction
$Y_{fu,inf}$	mass fraction of fuel at infinity; taken as 1.0

* Corresponding author. Current address: Institute of Chemical Engineering and High Temperature Chemical Processes, PO Box 1414, 26500 Patras, Greece.

COMBUSTION AND FLAME 109: 198–223 (1997)

Published by Elsevier Science Inc.

0010-2180/97/$17.00
PII S0010-2180(96)00149-6

$Y_{ox,inf}$ mass fraction of oxygen at infinity; taken as 0.233

Greek

γ ratio of specific heats; Section 2.1
δ characteristic initial thickness of the fuel–air interface
Δt_{df} estimate of time for diffusion flame complete ignition; Section 3.3
ϵ dissipation rate of the turbulent kinetic energy
η_K Kolmogorov length scale
ν dynamic viscosity
ρ density
τ_{ign} time of first appearance of autoignition in laminar and turbulent mixing layers
τ_{hom} autoignition time of homogeneous, stagnant, adiabatic mixtures
τ_{ref} minimum τ_{hom}; Section 3.1 and Fig. 2
τ_{turb} turbulent integral time scale; Section 2.2
ϕ mass ratio of oxygen to fuel at stoichiometry
χ scalar dissipation rate; Eq. 8
$\chi|f$ scalar dissipation rate conditional on the mixture fraction being f

Subscripts

fu quantity at the fuel stream
ign first appearance of autoignition
MR most reactive (for the mixture fraction)
ox quantity at the oxidant stream
st stoichiometric
turb turbulent integral scale

Other

$\langle\ \rangle$ volume average
$\psi|f$ property ψ conditional on the mixture fraction taking the value f

1. INTRODUCTION

The autoignition of hydrocarbon fuels following their release inside a turbulent oxidant at elevated temperature is relevant to combustion in diesel and aircraft jet engines. Despite the importance of these applications, detailed understanding of the time and spatial location of, and the subsequent flame development from, autoignition sites is still lacking. For example, recent visualisations in diesel engines by Baritaud et al. [1] have shown that the ignition spots were scattered in a region on the order of the spray width, but were located mostly on the sides of the spray, in contrast to other experiments [2] that showed ignition at the spray tip. The autoignition times, determined as the time of first appearance of intense light inside the cylinder, also showed large scatter. These observations are important for the accurate representation of autoignition in numerical field solutions of the flow inside the engine, used routinely now as design tools [3].

It is not well understood why sprays autoignite on the side—probably in lean regions —and neither is there a satisfactory explanation of the relationship between the autoignition time observed in experiments where the fuel–air mixture is inhomogeneous, as in sprays [4], and in experiments with homogeneous mixtures in shock tubes [5]. Finally, experimental evidence [1, 6] shows that increased turbulence may reduce the autoignition time which is, at first, counterintuitive based upon laminar flow analyses [7–9] that suggest that the high strain rates caused by high turbulence will delay autoignition and may even totally prohibit it.

In an effort to understand these problems better, autoignition in laminar and turbulent mixing layers was examined with two-dimensional direct numerical simulations (DNS) with one-step chemistry. In particular, the objectives of the present work were (i) to quantify the autoignition time in turbulent flows relative to that in homogeneous, adiabatic, stagnant mixtures, (ii) to measure with DNS the randomness involved in the first appearance of autoignition spots, (iii) to quantify the effect of the turbulence and of the initial length scale of the fuel stream on the autoignition time, and (iv) to identify the spatial distribution of ignition sites. It is found that ignition is located in regions with a specific value of the mixture fraction and with low values of the scalar dissipation rate and so, with hindsight, we may also consider as an aim (v) to conjecture on proper modelling approaches for the autoignition of inhomogeneous mixtures.

This paper is organised as follows. In the next section, the numerical methods are described and the results are presented in Section 3. First, the autoignition of homogeneous mixtures is described as a "reference" situation and is followed by a discussion on the autoignition of turbulent mixing layers in Section 3.2. Some preliminary findings on the establishment of the whole diffusion flame following autoignition are shown in Section 3.3 and results for turbulent flows with fuel streams of finite extent are given in Section 3.4, to identify the influence of length scale on autoignition. The implications of the present results are discussed in Section 3.5 and the main conclusions are summarised in Section 4.

2. NUMERICAL METHODS

2.1. The Code

A two-dimensional code with simple one-step chemistry and incorporating realistic heat release, as described in Refs. 10 and 11, has been used. The code solves nondimensional versions of the continuity, momentum, energy, and two species conservation governing equations in fully compressible form. It uses temperature-dependent molecular transport coefficients and assumes constant and uniform molecular weight, specific heat, Prandtl and Schmidt numbers, and ratio of specific heats γ. In this work, $\mathrm{Pr} = \mathrm{Sc} = 0.7$ and $\gamma = 1.4$. The only other parameter that appears in the nondimensional governing equations is the Reynolds number Re, defined as $c_{\mathrm{ref}} L_{\mathrm{ref}}/\nu$, with c_{ref} the velocity of sound at a reference state, L_{ref} a characteristic length scale, and ν the kinematic viscosity. Because the reference velocity is the sound velocity, the Reynolds number so defined may be called "acoustic" and the time scale defined by $t_{\mathrm{ref}} = L_{\mathrm{ref}}/c_{\mathrm{ref}}$ is referred to as "acoustic time." In this work we chose $\mathrm{Re} = 10^5$ and the reference state to be air at atmospheric conditions to give the reference quantities $c_{\mathrm{ref}} = 347.67$ m/s for velocities, $L_{\mathrm{ref}} = 4.37$ mm for lengths, and $t_{\mathrm{ref}} = 1.259 \times 10^{-5}$ s for times. Note that, for the purposes of this work, these numbers are not of any consequence since we compare the autoignition times in turbulent flows with those in homogeneous mixtures and both are nondimensionalised by the same quantities.

2.2. Initial and Boundary Conditions

2.2.1. Initial Scalar Distributions and Chemical Parameters

A 251×251 grid for all the turbulent flow data and a small 10×10 grid for the homogeneous stagnant mixture calculations were used. All grids had uniform spacing and the solution domain had length $L_{\mathrm{box}} = L_{\mathrm{ref}}$ in both directions. For all calculations, the initial pressure in the solution domain was taken as uniform and equal to $P = 1$ atm and the initial reaction rate was zero. The initial values of species mass fractions, temperature, and density were determined as in inert flow by a specified spatial distribution of the mixture fraction by the following relationships:

$$Y_1 = Y_{\mathrm{fu,inf}} f, \tag{1}$$

$$Y_2 = Y_{\mathrm{ox,inf}} (1 - f), \tag{2}$$

$$T_{\mathrm{in}} = T_{\mathrm{ox}} - f(T_{\mathrm{ox}} - T_{\mathrm{fu}}), \tag{3}$$

$$\rho = \frac{P}{RT}, \tag{4}$$

where f, the mixture fraction, is defined by

$$f = \frac{\phi Y_1 - Y_2 + Y_{\mathrm{ox,inf}}}{\phi Y_{\mathrm{fu,inf}} + Y_{\mathrm{ox,inf}}}. \tag{5}$$

The stoichiometry of methane was used to give a mass ratio of stoichiometric O_2/CH_4 mixtures ϕ equal to 4; $Y_{\mathrm{ox,inf}} = 0.233$ and $Y_{\mathrm{fu,inf}} = 1.0$ throughout and so the stoichiometric mixture fraction was $f_{\mathrm{st}} = 0.055$. Equation 3 is valid because the molecular diffusivities of mass and temperature are taken to be equal. For all calculations, T_{fu} was taken as 300 K and T_{ox} as 1000 or 1100 K. The activation energy of the one-step reaction, first order to each reactant, was 14,400 K, which is lower than the value of 24,356 K recommended by Westbrook and Dryer [12] in order to make the governing equations less stiff, but high enough to ensure sudden ignition, a characteristic of high-activation energy reactions. The preexponential factor was taken as 4×10^{11} 1/s, chosen arbitrarily to ensure ignition in a conveniently short time to reduce computational cost.

The heat release per unit mass of fuel Q was taken as 41,640 kJ/kg.

For mixing layer calculations (Fig. 1a), the initial distribution of mixture fraction in a thin interface separating fuel ($f = f_o$) and air ($f = 0$) is given by

$$f = f_o \frac{1}{2}\left[1 - \mathrm{erf}\left(\frac{x - x_o}{\delta}\right)\right] \tag{6}$$

in the inhomogeneous direction. It is uniform in the y direction. In Eq. 6, δ is a characteristic scale of the width of the error-function profile, x_o is the location of the midpoint of the profile, and f_o is the maximum value of the mixture fraction in the fuel stream. The value of x_o was taken as 0.5, i.e., the midpoint of the solution domain (Fig. 1). The value of f_o determines the amount of partial premixing in the fuel stream and $f_o = 1$ (100% fuel) and $f_o = 0.5$ (50% CH_4/50% air by mass) have been used. An error-function interface is consistent with the solution to the one-dimensional unsteady diffusion equation.

2.2.2. Initial Velocity Field

The initial cross-layer mean velocity was determined by an approximate form of the integrated steady energy equation [13]. Tests, however, showed that the results of interest here are similar even if the initial cross-layer veloc-

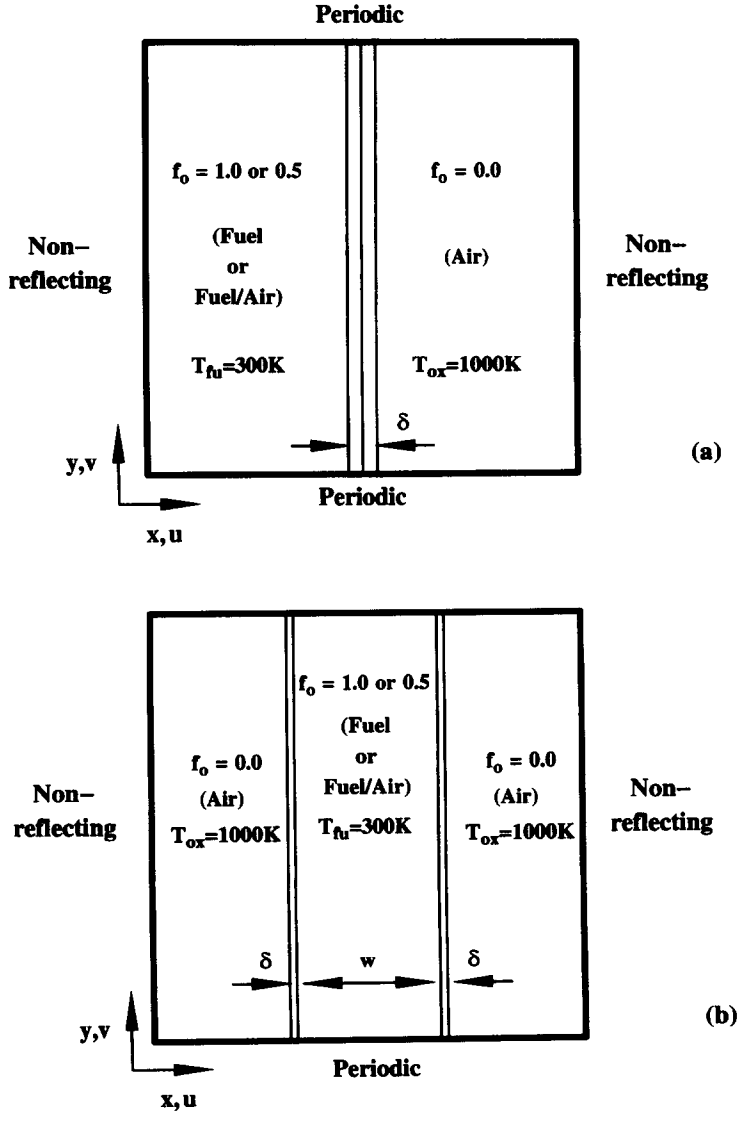

Fig. 1. Flow arrangement for (a) infinite layers and (b) slab calculations.

ity was zero and so this aspect of initialisation is of no consequence. Zero mean velocities were employed along the homogeneous direction (y). Initialisation of the turbulent velocity fluctuations, which were added to the mean velocities imposed, was performed in the manner described in Ref. 14 with an energy spectrum with the scale of the most energetic eddies k_e and the scale of the dissipative eddies k_d as parameters. The values of these wave numbers determine the initial turbulent kinetic energy k and its dissipation rate ϵ, and thus the turbulent integral length and time scales, defined here as $L_{\text{turb}} = k^{3/2}/\epsilon$ and $\tau_{\text{turb}} = k/\epsilon$, respectively. The turbulent Reynolds number Re_t, defined by $k^{1/2}L_{\text{turb}}/\nu$, had values between 60 and 100, from which the Kolmogorov length scale $\eta_K = L_{\text{turb}}\,\text{Re}_t^{-3/4}$ could be estimated. There is no forcing because it is not clear how energy should be fed into the turbulence in simulations with variable density and combustion, contrary to DNS of isothermal flows. Hence, the simulations presented here occur in a turbulent field which is decaying, but is known at all times.

2.2.3. Laminar and Slab Calculations

A few results on the autoignition of *laminar* mixing layers were obtained by a one-dimensional version of the code with initial condition also given by Eqs. 1–6. Turbulent calculations were also made of fuel streams of finite extent w, not infinite layers, where the two interfaces were located at $x_0 = 0.5 \pm w/2$ to show the effect of flow scale on autoignition time (Fig. 1b). Typically, $\eta_K \ll w < L_{\text{turb}}$.

2.2.4. Resolution

Important points concerning the resolution requirements of the simulations are that the smallest velocity and scalar scales should be resolved and that the turbulent integral length scale should be less than about 0.3 of the solution domain to avoid influence of the boundary conditions. Here, the solution domain had a (nondimensional) length of unity, L_{turb} varied between 0.05 to 0.20, and the minimum grid spacing was 1.32 times the Kolmogorov scale at worst. However, because the turbulence decays and the length scales grow quickly, because half the domain (the air side) is at a higher temperature and hence more viscous, and because simulations with better resolution gave identical results, we consider that the present simulations adequately resolve the velocity field.

Extra care was needed to resolve accurately the initial thin interface between the air and the fuel. Numerical problems associated with the steep density difference of the two streams arose when there were less than about six grid points across the interface, a more stringent requirement than that for the velocity field. There was a minimum value of δ that could be used for a given grid and, by trial and error, $\delta = 0.005$ was found to be the smallest that ensured good resolution for the present grid (which had a spacing of $\Delta x = 0.004$). Higher values, giving a wider interface, were also examined to quantify the influence of the initial value of δ on autoignition. Typically, $L_{\text{turb}} \gg \delta > \eta_K$.

2.2.5. Boundary and Flow Conditions

For all simulations, periodic boundary conditions in the y direction and nonreflecting boundaries [15] in the x direction were used, with the exception of the homogeneous mixture solutions, which were obtained with periodic conditions in both directions and no flow. Figure 1 shows schematically the initial geometry and Table 1 itemises some of the flow parameters tested. The times of first appearance of autoignition are also listed to facilitate later discussion. It is expected that the present two-dimensional simulations are adequate for examining the effect of real turbulence on autoignition because the main physical phenomena of the coupling between the chemical reactions, heat release, and flow field effects on mixing are, at least qualitatively, captured in two dimensions.

3. RESULTS AND DISCUSSION

3.1. Autoignition of Homogeneous Mixtures and τ_{ref}

The autoignition of stagnant adiabatic homogeneous mixtures is described in this section to show the influence of the initial temperature and concentration on the autoignition time.

TABLE 1

Flow Conditions for Some Typical Simulations and Resulting Autoignition Times τ_{ign}[a]

Run	Type	f_o	δ	w	τ_{turb}	L_{turb}	η_K	T_{ox} (K)	τ_{ign}/τ_{ref}
1	Layer	1.0	0.005	—	7.20	0.070	0.003	1100	2.566
2	Layer	1.0	0.010	—	7.20	0.070	0.003	1100	2.391
3	Layer	0.5	0.010	—	7.20	0.070	0.003	1100	2.250
4	Slab	0.5	0.005	0.050	7.20	0.070	0.003	1100	2.297
5	Slab	0.5	0.005	0.050	7.20	0.070	0.003	1000	2.180
6	Slab	0.5	0.005	0.025	7.20	0.070	0.003	1000	1.919
7	Slab	0.5	0.005	0.025	4.22	0.053	0.002	1000	1.916

[a]For all, T_{fu} = 300 K. See Section 3.1 for the definition of ignition time scale τ_{ref}. All lengths have been nondimensionalised by the reference length scale L_{ref}, but because in all simulations $L_{box} = L_{ref}$, these lengths can be thought of as normalised by the solution domain size. Note also that the turbulence time τ_{turb} is in units of the "acoustic time" t_{ref}.

This will also provide a reference against which the subsequent results in inhomogeneous and turbulent mixtures can be compared.

Consider adiabatic homogeneous mixtures with no flow, with initial composition and temperature related by Eqs. 1–3, hence uniquely characterised by the mixture fraction. The autoignition times τ_{hom} of these mixtures have been found and are presented in Fig. 2. This shows that τ_{hom} has a minimum value for a mixture fraction of about 0.11, for both oxidant temperatures tested. The minimum values, denoted by τ_{ref}, were 6.309 and 2.194 for T_{ox} = 1000 and 1100 K, respectively. These autoignition times depend only on the initial state of the mixture and the chemistry used, not on the flow. Thus they can be used as "reference" times with which the results of the turbulent flows examined in the next sections can be compared. The existence of a minimum au-

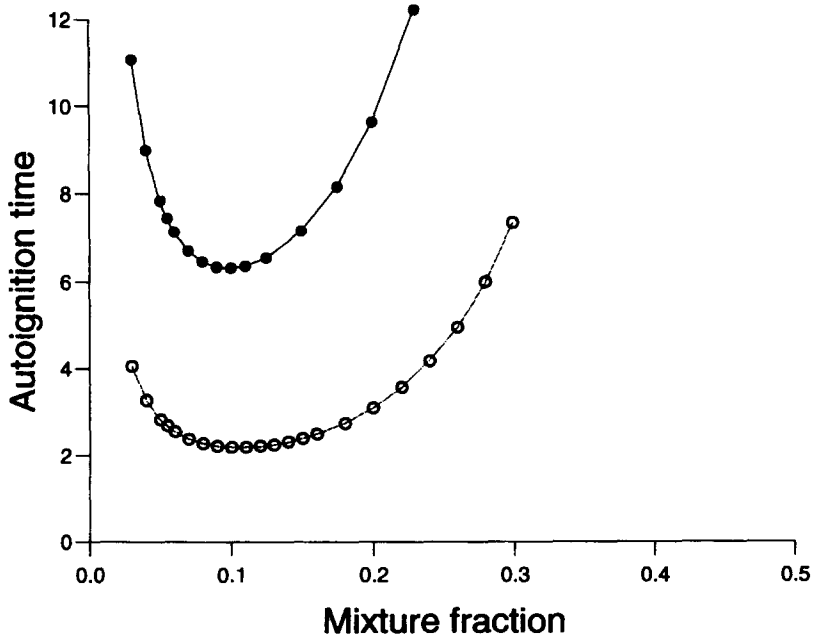

Fig. 2. Autoignition times of homogeneous, adiabatic, stagnant mixtures with initial composition and temperature related by Eqs. 1–3, for T_{ox} = 1000 (solid circles) and 1100 K (open circles). The minimum value τ_{ref} is used in the text for comparisons with autoignition times of *inhomogeneous* turbulent mixtures.

toignition time suggests that there is an optimum mixture fraction for faster ignition. It is explained by the fact that toward lean mixtures, the beneficial effect of the high initial temperature more than compensates for the reduced fuel concentration because of the exponential dependence of the reaction rate on temperature.

It is important to realise that in any flow with initially separate fuel and air streams, fluid particles will have concentrations and temperatures uniquely determined by the mixture fraction for a time short compared to the ignition time, that is, before appreciable reaction has increased the temperature or decreased the reactant concentrations. It is not possible for the temperature and concentration to be independent. Therefore the results of Fig. 2 can also be interpreted as follows: in an infinitely fast mixing flow between hot air and cold fuel, depending on the amount of the two reactants, the final mixture formed will have a concentration and temperature determined by the final value of the mixture fraction. The subsequent autoignition will then be a function of *this* mixture fraction, the ignition time will follow the results of Fig. 2, and thus τ_{ref} can be considered as the *minimum possible autoignition time of mixtures* created by fuel and oxidant streams of given initial temperatures. Thus Fig. 2 provides a characteristic time scale of the chemistry. The delaying effect of inhomogeneities present during the time to ignition (induction time) in turbulent mixing flows is measured by the ratio of the ignition time to τ_{ref} and forms the topic of this work.

3.2. Autoignition of Turbulent Mixing Layers

Results on the autoignition of mixing layers in an initially isotropic and homogeneous velocity turbulent field are presented here. First, a typical sequence of events before, during, and after autoignition is described and the calculations are then used to visualise the spatial distribution of the ignition sites. The random nature of the ignition time and its dependence on the turbulence time scale are then presented and discussed.

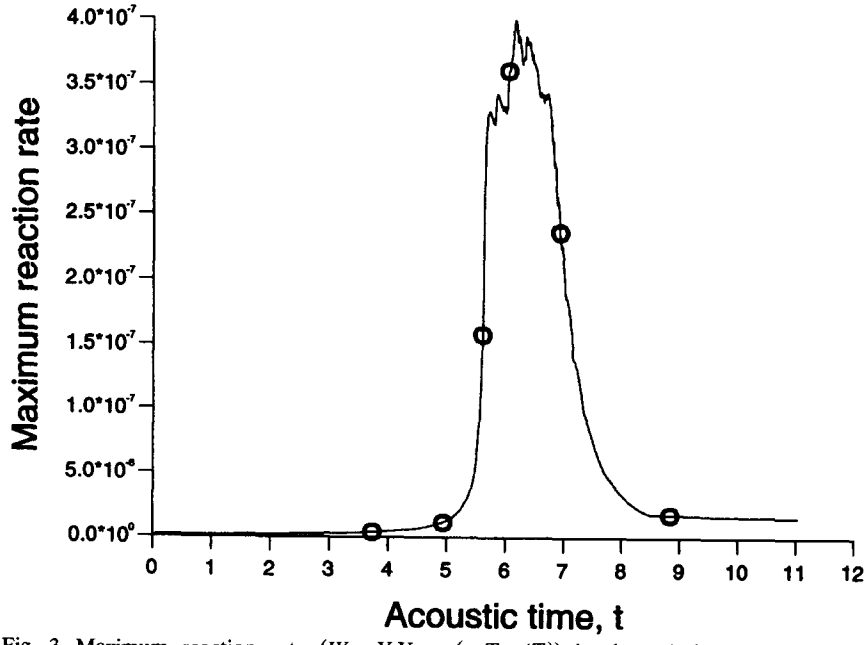

Fig. 3. Maximum reaction rate ($W = Y_1 Y_2 \exp(-T_{act}/T)$) in the solution domain as a function of acoustic time for the simulation denoted as RUN1 in Table 1. Circles on the curve denote the times of the data in Figs. 5–8.

3.2.1. A Typical Sequence

Figure 3 shows that the maximum reaction rate in the solution domain increases very sharply after a period of slow increase; the point of maximum gradient in this sharp increase defines the autoignition time. Figure 4 shows the corresponding trace of the volume-averaged pressure which rises after ignition, but with a slightly longer delay compared to the reaction rate. Solid circles on Fig. 3 mark times where two-dimensional contours of mixture fraction, temperature, and reaction rate have been assembled and these are presented in Figs. 5–7. Recall that the initial state of the flow had $f = 1.0$ and $T = 300$ K (i.e., pure fuel) on the left side of the straight interface, located at the midpoint of the domain, and $f = 0.0$ and $T = 1100$ K (i.e., pure air) on the right side. Note that autoignition occurs at about 0.8 (initial) turbulent time scales.

As time evolves, the interface develops wrinkles due to the turbulence and becomes more diffuse due to the combined action of small eddies and molecular diffusion (Fig. 5, first column). Ignition occurs just after the snapshot at $t/\tau_{\text{turb}} = 0.78$ in Fig. 5, and it is evident that after ignition the mixing layer expands in the inhomogeneous direction. At $t/\tau_{\text{turb}} = 0.78$, the temperature has not risen much from its inert value (Fig. 6), although a small increase is observable on the lean side of the layer. At $t/\tau_{\text{turb}} = 0.84$, after autoignition, only two isolated regions have high temperatures; therefore autoignition is *localised.* These high-temperature regions spread and merge with other autoignition spots to form a connected (in the y direction) zone (at $t/\tau_{\text{curb}} = 0.97$) and then the maximum reaction rate in the domain, which is associated with igniting elements, begins to fall.

The expansion of the high-temperature regions is made clear by examining the reaction rate contours in Fig. 7. Long before ignition, the reaction rate is low and follows approximately the lean mixture fraction contours. Just before ignition, high reaction rates are localised at two spots which are clearly the ones that have ignited at $t/\tau_{\text{turb}} = 0.84$. Figure 7 at $t/\tau_{\text{turb}} = 0.84$ is important for the qualitative understanding of the flame establishment after autoignition. Following ignition at a point, the reaction rate drops there to zero because one

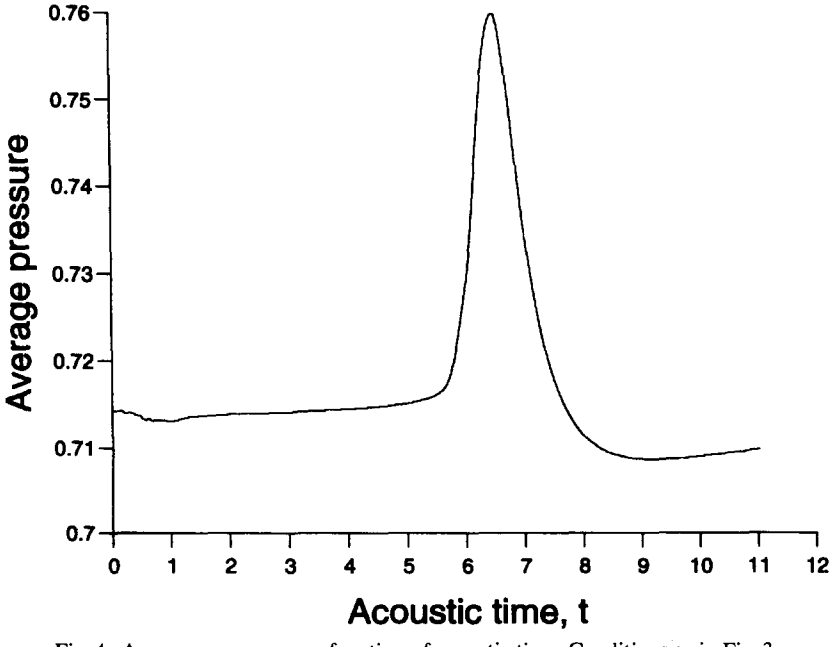

Fig. 4. Average pressure as a function of acoustic time. Conditions as in Fig. 3.

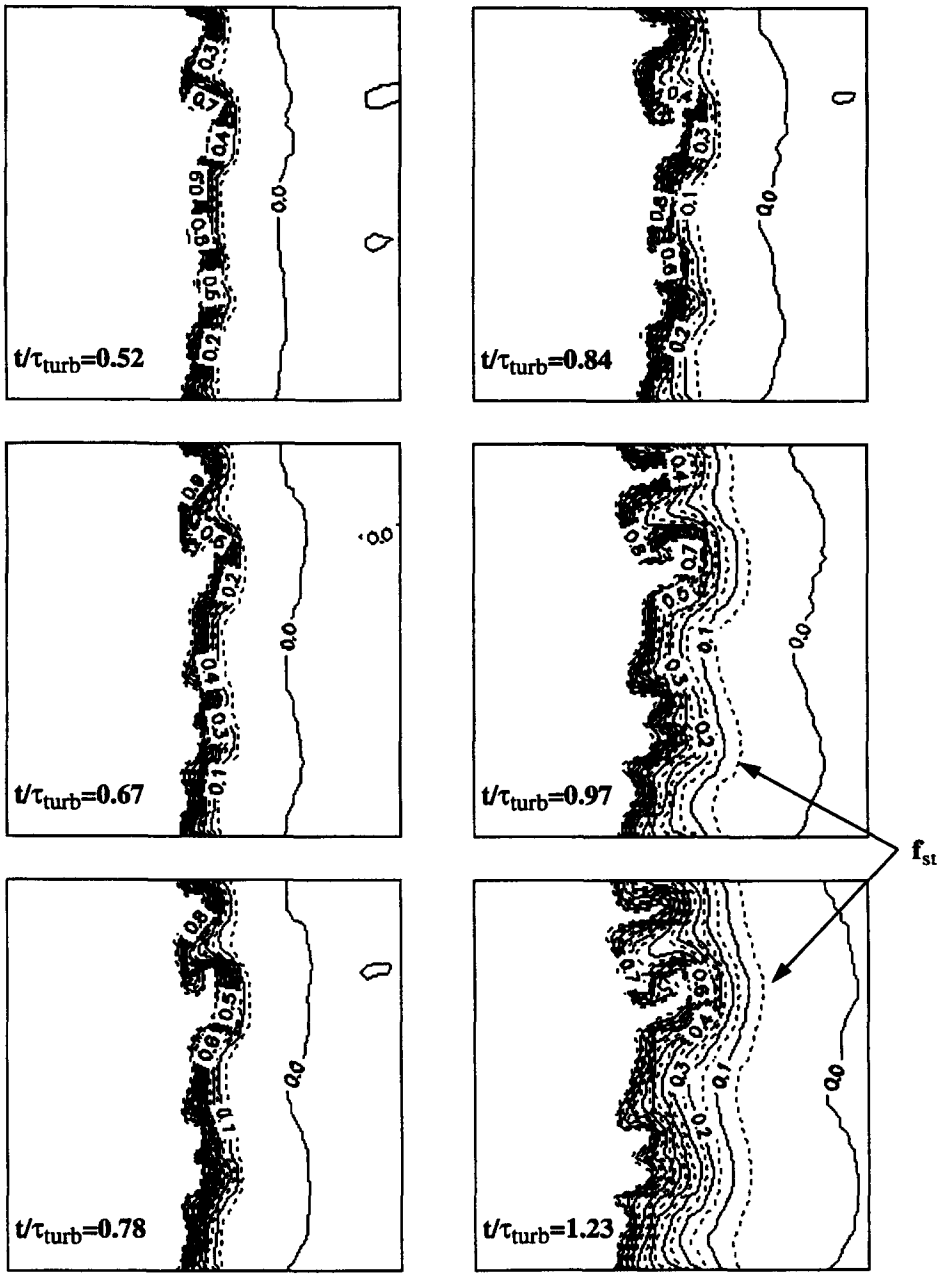

Fig. 5. Contours of mixture fraction, for times before and after autoignition for RUN1. Ignition first observed at $\tau_{ign} = 5.631$, i.e., $\tau_{ign}/\tau_{turb} = 0.782$.

or both reactants have been consumed, forming hence an "island" of high-temperature fluid centred on the ignition spot surrounded by a circular reaction front. These circular reaction fronts propagate outward and collapse at the very lean or very rich sides due to extinction or after collisions with separate similar fronts originating from other ignition sites. Note the development of additional autoignition locations at $t/\tau_{turb} = 0.84$, later than the first appearance of autoignition. Much later (the plot at $t/\tau_{turb} = 1.23$), a continuous reaction front at the stoichiometric mixture fraction has been created (the "diffusion" flame), a weak and

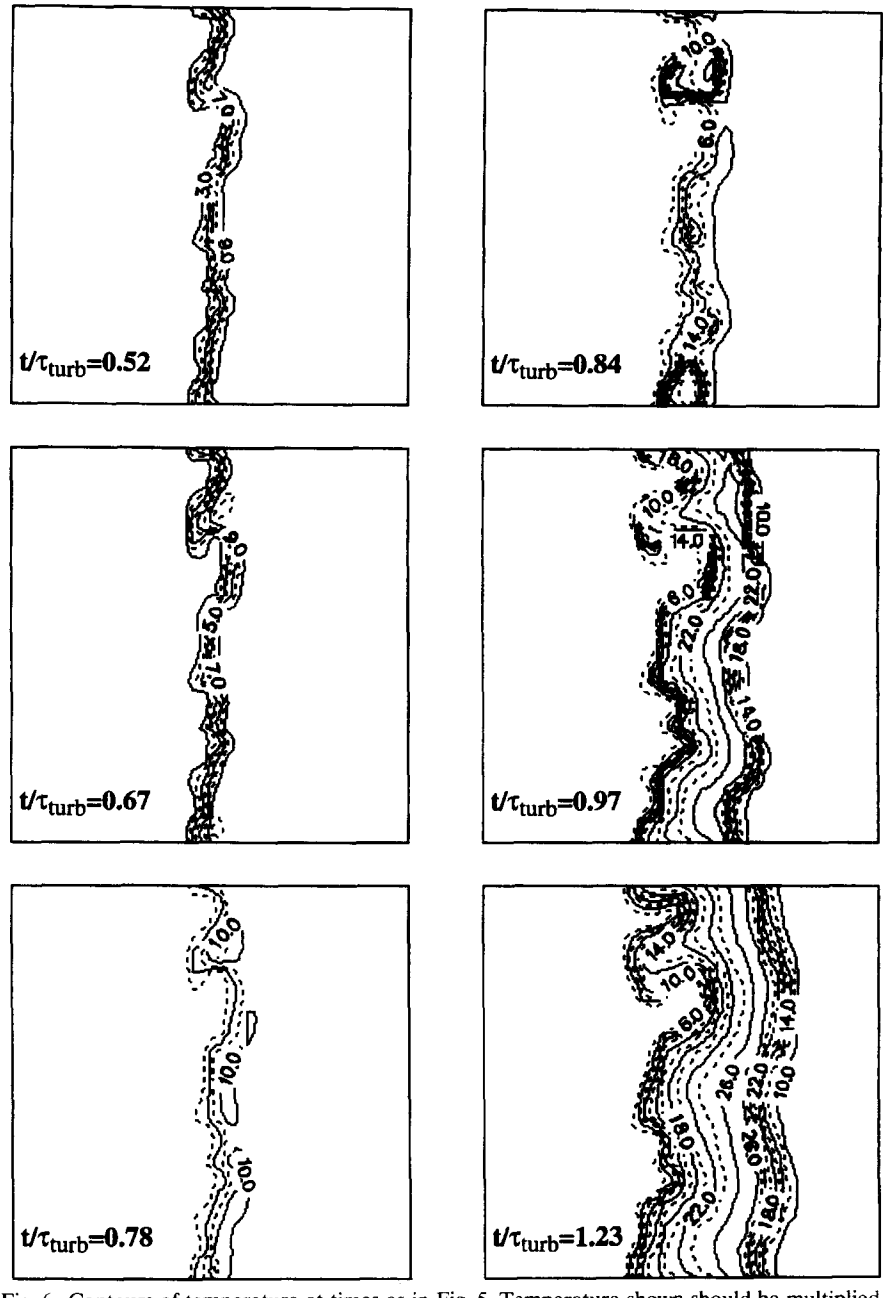

Fig. 6. Contours of temperature at times as in Fig. 5. Temperature shown should be multiplied by 120 to give kelvin.

decaying front at leaner mixtures is still propagating, and a stronger front is still evident at rich mixtures.

Finally, we show in Fig. 8 scatter plots of the reactedness against the mixture fraction. The reactedness b is defined by

$$b = \frac{(T - T_{\text{in}})}{\Delta T_{\text{ad}}}, \tag{7}$$

where $\Delta T_{\text{ad}} = f_{\text{st}} Q / c_p$ is the temperature in-

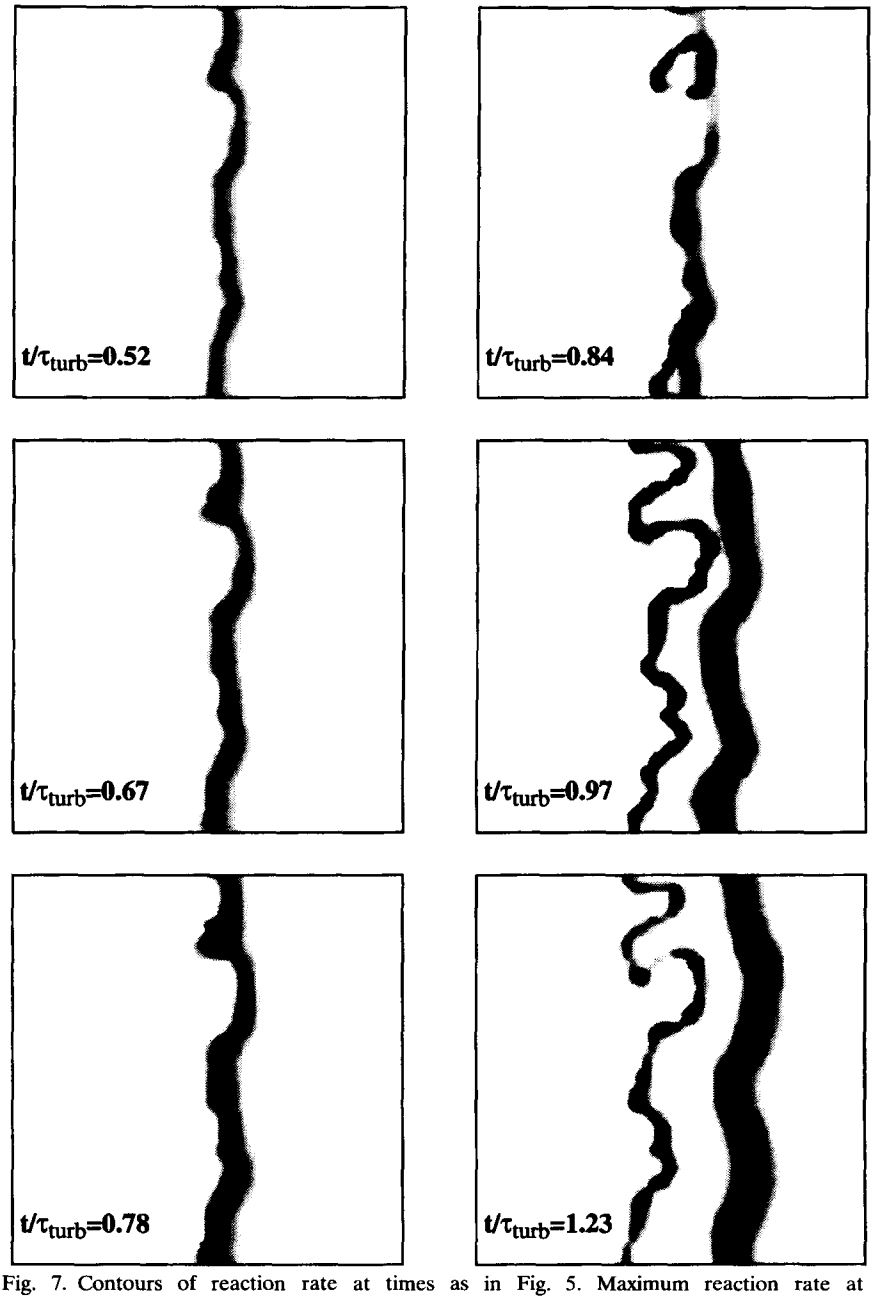

Fig. 7. Contours of reaction rate at times as in Fig. 5. Maximum reaction rate at $t/\tau_{turb} = 0.84$ in 10 times higher than in other plots. Black corresponds to high values; white corresponds to zero.

crement due to reaction in a stoichiometric adiabatic flame, with Q the heat release per unit mass of fuel and c_p the specific heat capacity, and T_{in} is the temperature corresponding to inert mixing (the initial value at $t = 0$) and determined by the local value of the mixture fraction through Eq. 3. With this definition, b is zero initially, rises slowly before autoignition, becoming unity when fully burnt for the stoichiometric mixture fraction, and decreasing linearly to zero at the air and fuel side. It is evident from Fig. 8 that the temperature increases little before autoignition, while later, the reactedness approaches the fully

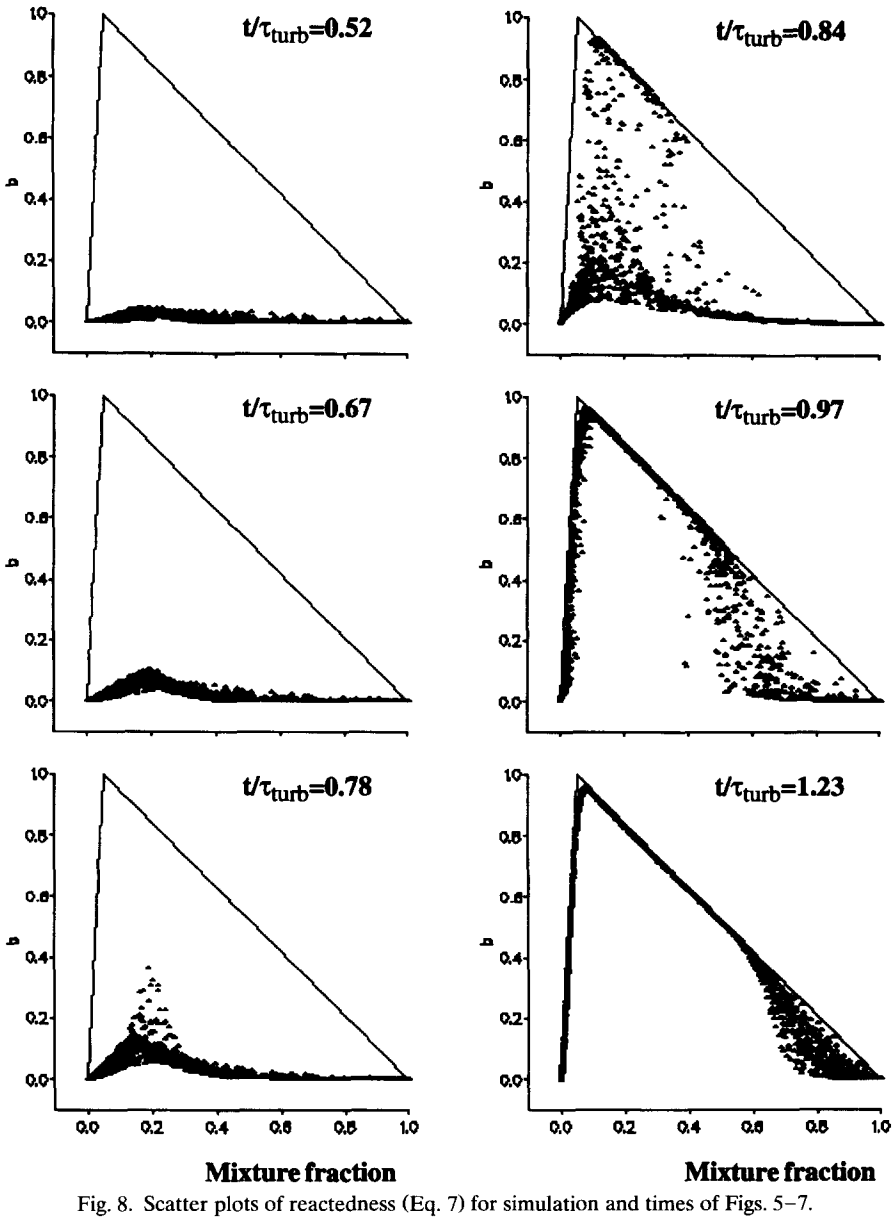

Fig. 8. Scatter plots of reactedness (Eq. 7) for simulation and times of Figs. 5–7.

burnt value, but with large scatter. There is evidence of unreacted very rich and very lean fluid long after ignition because the propagation speed of the fronts of Fig. 7 approaches zero when the concentration of one of the two reactants becomes very low.

This scenario of autoignition has been observed for all initial layer thicknesses, oxidant temperatures, fuel premixedness, and turbulent time scales tested, although the ignition time varies. The results are consistent with the conclusions of Liñan and Crespo [16], reached by asymptotic methods, and of Thevenin and Candel [7], obtained by constant-density numerical solutions for one-dimensional laminar autoigniting layers, that reaction fronts propagate toward lean and rich mixtures after ignition. When these reaction fronts "cross" regions with stoichiometric mixture fraction, the "diffusion" flame is ignited and an estimate of

the time difference between ignition and the establishment of the diffusion flame is given in Section 3.3. In the next section, the difference between the igniting and the stoichiometric mixture fractions is emphasised.

Qualitatively, the simulations show that the transition from frozen flow to diffusion-type reacting flow after autoignition occurs over a finite time, during which rich mixtures are reacting slowly and thus possibly creating pollutants. Also note that reaction takes place not only at stoichiometry, but also at richer locations, and so the fuel that has been premixed with oxygen during the induction time can be consumed at either. The common deficiency of some diesel engine calculations to underpredict fuel burnout may thus be explained as they usually neglect this mode of "premixed" combustion [17].

3.2.2. Location of Autoignition Sites

We examine below in detail the spatial distribution of the autoignition sites and conclude that they are associated with a particular value of the mixture fraction, to be denoted as the "most reactive" $f_{MR} = 0.12$, and with low values of the scalar dissipation rate.

It was evident from Fig. 8 that the reactedness was highest in a small region of mixture fraction around 0.1–0.15 before autoignition, and this suggests that *these* mixture fractions first ignite. In more detail, Fig. 9 shows that the reaction rate, conditionally averaged in small "windows" of mixture fraction, peaks at around 0.12 for most of the time until ignition and falls sharply at leaner and richer mixtures. We call the mixture fraction at the highest reaction rate f_{MR}. The value of f_{MR} did not change in simulations with different initial values of δ and turbulence intensity, but f_{MR} was altered by changing T_{ox} and/or T_{fu} and this is discussed in Section 3.5. It is clear that autoignition occurs in sites with $f = f_{MR}$, but it is not evident which portions of the f_{MR} contour are preferred.

Motivated by the known dependence of the ignition time on heat losses during the induction period and by the expectation that large gradients of mixture fraction imply large heat losses, we examine below the (nondimensional)

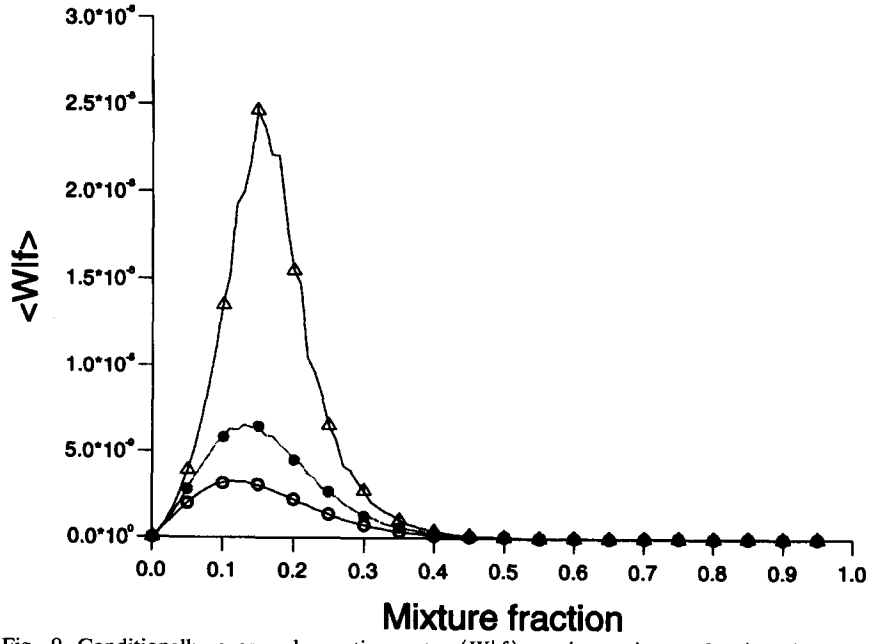

Fig. 9. Conditionally averaged reaction rate $\langle W|f \rangle$ against mixture fraction for the simulation of Figs. 5–8, before autoignition at $t/\tau_{turb} = 0.52$ (open circles), 0.67 (solid circles), and 0.78 (triangles).

scalar dissipation rate, defined by

$$\chi = \frac{1}{\mathrm{Sc}}\left[\left(\frac{\partial f}{\partial x}\right)^2 + \left(\frac{\partial f}{\partial y}\right)^2\right]. \quad (8)$$

To obtain dimensional values, the presented χ should be divided by $\frac{1}{2}\,\mathrm{Re}\,t_{\mathrm{ref}}$ (see Section 2.2).

Figure 10 shows scatter plots of the reaction rate against the scalar dissipation rate, but conditioned on the mixture fraction being in the range $0.11 < f < 0.14$, bracketing f_{MR}. It is evident that the reaction rate is low when χ is large and high when χ is low for the most reactive fluid elements and that this is so for all times until autoignition. The strong negative correlation between the reaction rate and the conditional scalar dissipation rate is shown in more detail in Fig. 11 as a function of mixture fraction. The conditional correlation coefficient between the reaction rate and the scalar dissipation rate fluctuations is negative and peaks at almost -1 at $f = f_{\mathrm{MR}}$.

The result of Figs. 9 and 11 and the observations in the scatter plots of Figs. 8 and 10 lead to the most important conclusion of the present work: autoignition in inhomogeneous mixtures is located where the mixture fraction assumes its most reactive value $f = f_{\mathrm{MR}}$ and where the conditional scalar dissipation rate $\chi|f_{\mathrm{MR}}$ is low. This behavior can be understood by considering that regions with high χ will have large heat losses, while regions with low χ will have low heat losses during the induction time. Since $\chi|f_{\mathrm{MR}}$ changes with time and also depends on the initial conditions and the turbulence intensity, we may expect that the time of the first appearance of autoignition can be related to the value of $\chi|f_{\mathrm{MR}}$. This dependence is discussed below and in Section 3.4, while a discussion of f_{MR} is given in Section 3.5.

3.2.3. Randomness of τ_{ign} and the Effect of τ_{turb}

No mention has yet been made of the values of the autoignition times and how these are affected by the turbulence. In particular, one prominent question posed in the Introduction was the randomness of τ_{ign}, which, based on

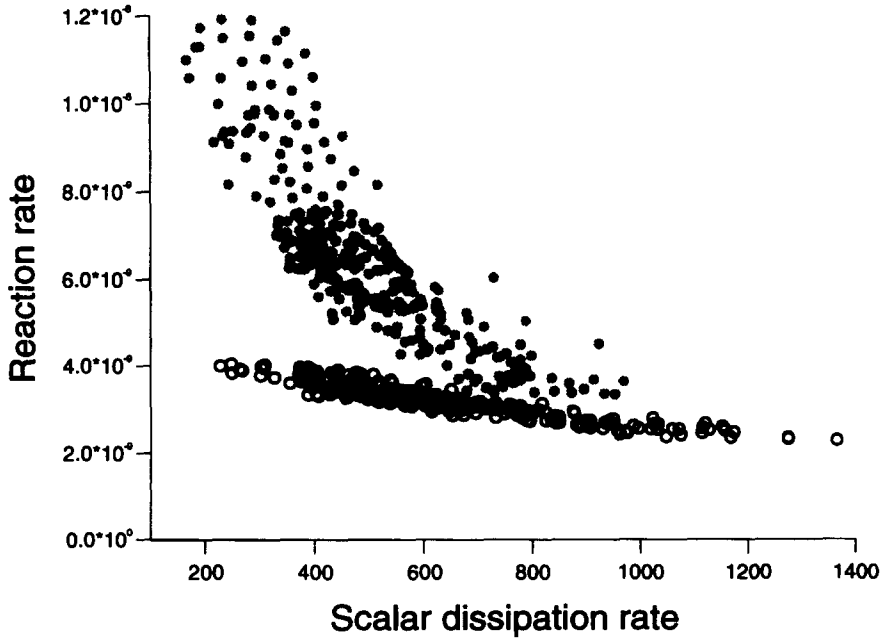

Fig. 10. Conditional scatter plots of reaction rate against scalar dissipation rate for $0.11 < f < 0.14$ before autoignition for RUN1. Open symbols for $t/\tau_{\mathrm{turb}} = 0.52$ and solid symbols for $t/\tau_{\mathrm{turb}} = 0.67$.

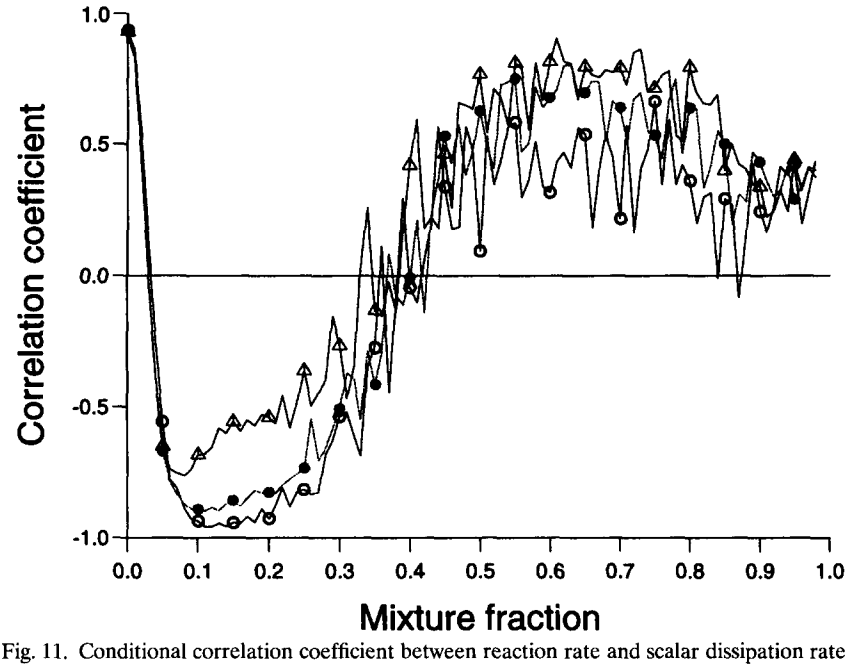

Fig. 11. Conditional correlation coefficient between reaction rate and scalar dissipation rate against mixture fraction for RUN1. Symbols and times are in Fig. 9.

the results of Section 3.2.2, must depend on the scalar dissipation rate conditioned on the most reactive mixture fraction. Since in a turbulent flow we expect (and indeed observe) large random variations of $\chi|f_{MR}$ that should depend on τ_{turb}, we intuitively expect a large randomness in τ_{ign} and a strong dependence on τ_{turb}. The following text shows that neither is true and explains why.

Figure 12 shows calculated autoignition times τ_{ign} from many simulations covering a range of τ_{turb}/τ_{ref} between about 0.8 and 15. Also included are results obtained by numerous realisations of the same flow (points aligned in the

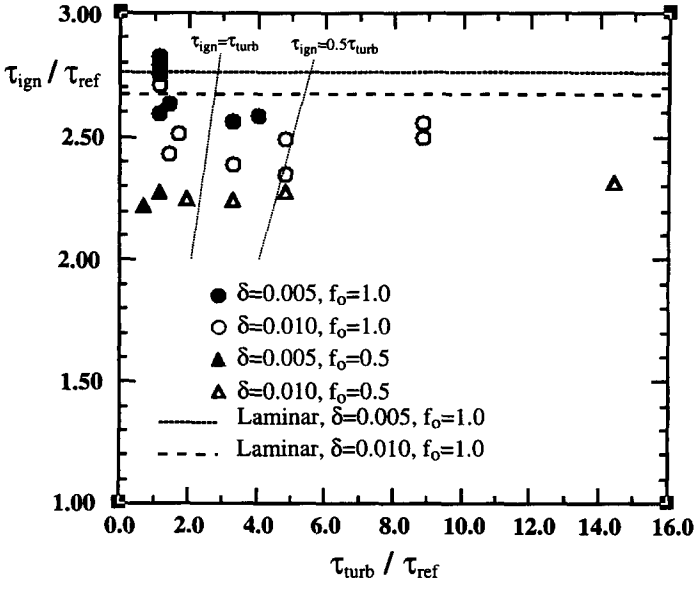

Fig. 12. Autoignition time normalised by the minimum ignition time of stagnant adiabatic mixtures τ_{ign}/τ_{ref} plotted against τ_{turb}/τ_{ref} for many simulations with different initial δ, T_{ox}, and τ_{turb}. Included are results of different realisations of the same flow (points vertically aligned) and results from one-dimensional *laminar* layer calculations with the same initial condition.

vertical direction in Fig. 12), of layers where the fuel stream is partially premixed with air at $f_o = 0.5$, of layers with different initial thickness δ of the fuel–air interface, and of *laminar* mixing layer calculations. The following conclusions, also evident from the results in Table 1, can be reached:

(a) Partially premixed flows ($f_o = 0.5$) ignite earlier than flows without partial premixing ($f_o = 1.0$).
(b) Increasing δ results in earlier ignition.
(c) The spread of autoignition times in different realisations of the same flow is small at large τ_{turb}/τ_{ref} and increases to about 10% at τ_{turb}/τ_{ref} close to unity.
(d) τ_{ign}/τ_{ref} is larger than unity and varies between 1.8 and 2.8, depending on the initial values of δ and f_o.
(e) τ_{ign} does not seem to depend on τ_{turb} by an amount larger than the spread between individual realisations.
(f) Turbulent flows ignite earlier than laminar ones.

These results are explained as follows. First, partial premixing implies smaller gradients of the mixture fraction for the same δ. Recall that the initial state of the mixing layer was, from Eq. 6, an error function spanning $f = 0$ in the air and $f = f_o$ in the fuel stream; a small value of f_o implies a smoother $\partial f/\partial x$ and thus χ at all times. Therefore partial premixing is a way to reduce the value of the scalar dissipation rate and hence the heat losses, and so the autoignition time is reduced.

Second, the dependence of the autoignition time on the scalar dissipation rate also explains why large values of δ (and hence low χ) result in short ignition delays. The effect of δ on ignition time is shown in more detail in Fig. 13 for both two-dimensional turbulent and one-dimensional laminar mixing layers (without turbulence). It is clear that increasing δ reduces the autoignition time.

Less expected is the result that turbulent flows ignite earlier than laminar one-dimensional flows of the same initial δ. This may at first seem counterintuitive as we expect turbulence, with the associated higher strain rates, to increase the ignition delay. We can understand it, however, if we recall from Fig. 10 that autoignition will occur at low $\chi|f_{MR}$ and by

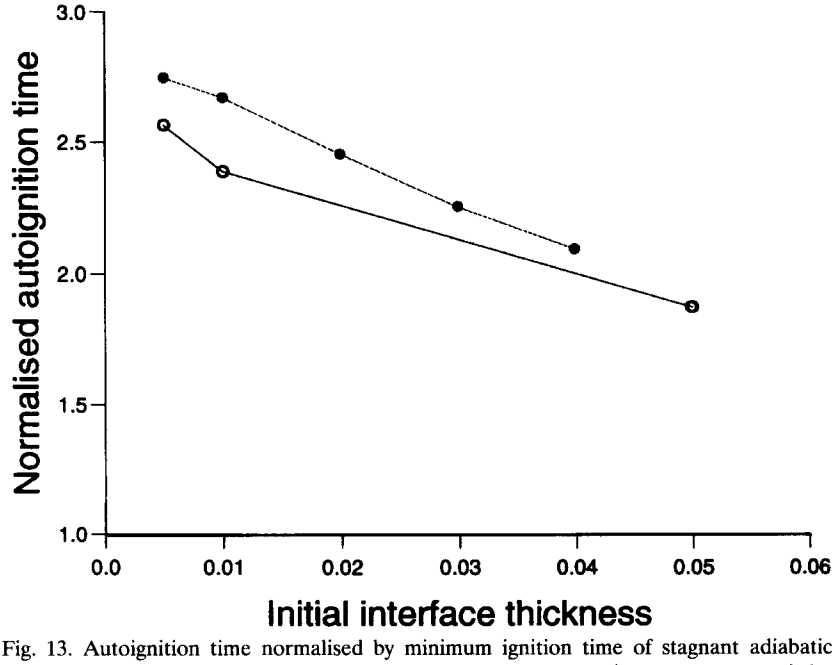

Fig. 13. Autoignition time normalised by minimum ignition time of stagnant adiabatic mixtures τ_{ign}/τ_{ref} as a function of initial δ for $T_{ox} = 1100$ K (giving $\tau_{ref} = 2.194$) for laminar one-dimensional calculations (solid circles) and turbulent flows (open circles). For turbulent flows, $\tau_{turb} = 7.20$ and $L_{turb} = 0.070$.

the expectation that turbulence creates a range of $\chi|f_{MR}$. Turbulence creates well-mixed spots, and hence with low $\chi|f_{MR}$ as well as highly strained regions, and hence with high $\chi|f_{MR}$. Because it is the former regions that favour autoignition and because turbulent mixing implies that the minimum value of $\chi|f_{MR}$ is smaller in a turbulent flow than in a laminar flow at the same time from the initial state, autoignition in the turbulent flow will be faster. This was also discussed on the basis of experimental results in Ref. 1.

The same argument explains the small dependence of the first appearance of autoignition on the turbulence time scale. It is expected that faster turbulence increases the mean and r.m.s. scalar dissipation rate for given mean scalar gradients. It is possible, however, that it alters but slightly the *minimum* values of $\chi|f_{MR}$ and, therefore, the autoignition time is not affected much by τ_{turb}.

Third, the small randomness of the first appearance of autoignition may again be understood by the result that autoignition occurs at the smallest values of the conditional scalar dissipation rate. It is *these* values that, if altered by some mechanism, also alter the autoignition time. Since it is likely that in any individual realisation of the flow the whole possible range of $\chi|f_{MR}$ and of its time evolution is encountered, it is also likely that the minimum values are also somewhere encountered. Autoignition will then occur at these sites and at the same time in different realisations, although at different locations in space. Therefore the small randomness measured in Fig. 12 is, in principle, due to the small statistical sample of $\chi|f_{MR}$ inside the solution domain, implying that if the domain were many turbulent length scales long, the observed randomness would be smaller. It may be expected that if $\tau_{ign} \gg \tau_{turb}$ (a condition not examined in detail here), significant variations may be developed in the history of $\chi|f_{MR}$ during the induction time. These may then cause the larger spread of the autoignition time in the region $\tau_{ign} > \tau_{turb}$ in Fig. 12. Note, however, that under the typical diesel engine conditions in Ref. 1, τ_{ign} was of the same order as τ_{turb} and so the results presented in Fig. 12 are relevant to engine practice.

Finally, the inequality $\tau_{ign}/\tau_{ref} > 1$ implies the presence of heat losses from the reactive regions of the flow and this gives credence to our conclusion that $\chi|f_{MR}$ controls autoignition in turbulent mixing flows.

3.3. Complete Ignition of the Nonpremixed Flame

Sections 3.2.1 and 3.2.2 showed that following autoignition at separate sites, reaction fronts propagate in all directions and eventually ignite fluid at the stoichiometric mixture fraction —the "diffusion" flame. The time needed for the establishment of a flame front, however, is finite and needs to be known for the accurate prediction of combustion in practical situations [3]. A quantification of this time is conjectured in this section.

Figure 14 shows that the conditionally averaged reactedness around f_{MR}, $\langle b|f_{MR}\rangle$, increases slowly before the first autoignition is observed (at $t = 5.631$ for the simulation shown). Following the first ignition, $\langle b|f_{MR}\rangle$ rises sharply and subsequently reaches its maximum value, close to the fully burnt temperature corresponding to f_{MR}. During this time the reactedness around f_{st}, $\langle b|f_{st}\rangle$, also rises, but less sharply, and there is a time delay until the conditionally averaged temperature of the *stoichiometric* fluid rises to the fully burnt value. Note that this value is less than the adiabatic flame temperature because the averages are made over windows in mixture fraction space of finite size. The time shift of the two curves in Fig. 14 provides direct evidence that the instant the diffusion flame is fully ignited occurs later than the time when all of the most reactive fluid has ignited, which in turn is longer than the first appearance of ignition τ_{ign}.

As a measure of the time delay for diffusion flame establishment, we measure the time shift between $\langle b|f_{MR}\rangle$ and $\langle b|f_{st}\rangle$[1] at the point of

[1] Although it would make more sense to define as the complete ignition of the diffusion flame the time where $\langle b|f_{st}\rangle$ has approached the fully burnt value, such a determination from the S-shaped $\langle b|f_{st}\rangle$ curve versus time is vague and so the midpoint of the curves was selected.

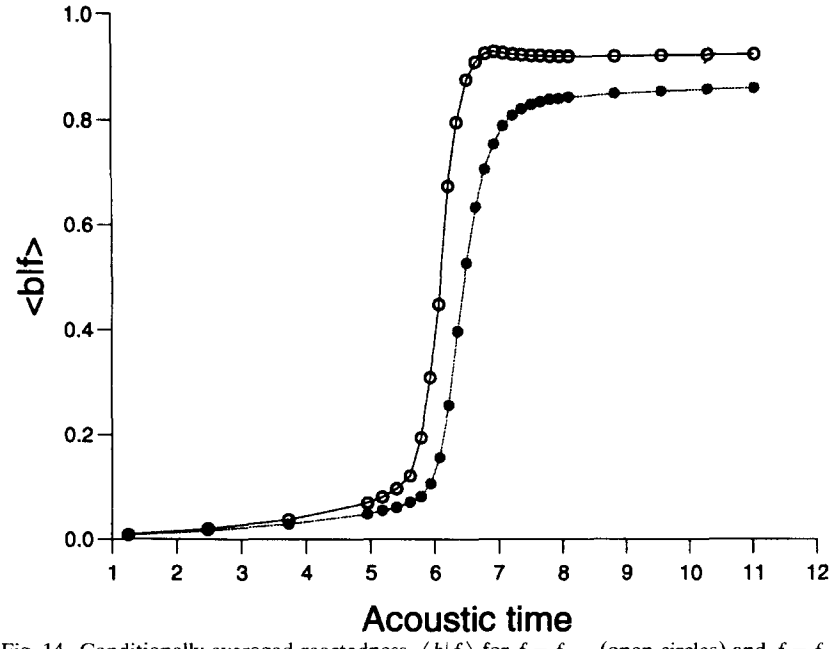

Fig. 14. Conditionally averaged reactedness, $\langle b|f \rangle$ for $f = f_{MR}$ (open circles) and $f = f_{st}$ (solid circles) plotted against acoustic time. The first appearance of autoignition for this simulation (RUN1) is at $t = 5.631$. The time lag between the two curves is Δt_{df}.

maximum gradient of curves like in Fig. 14. This time, Δt_{df}, should depend on the physical distance L_f between fluid of f_{MR} and f_{st} and on the propagation speed of the reaction fronts from the ignition to the stoichiometric mixture fraction, schematically shown in Fig. 15. An estimate of the distance between the f_{MR} and the f_{st} contour follows from the definition of the scalar dissipation rate:

$$L_f = (f_{MR} - f_{st})(\langle \chi|f_* \rangle / 2D_{mol})^{-1/2}, \quad (9)$$

where $\langle \chi|f_* \rangle$ is the average scalar dissipation rate conditional on $f_* = \frac{1}{2}(f_{MR} + f_{st})$ at the time of ignition. The quantity S_{df}, defined by

$$S_{df} = \frac{(f_{MR} - f_{st})(\langle \chi|f_* \rangle / 2D_{mol})^{-1/2}}{\Delta t_{df}}, \quad (10)$$

has the units of velocity and is a measure of the average propagation speed of the reaction fronts from the ignition sites to the stoichiometric mixture fraction (with the terms in Eqs. 9 and 10 in dimensional form). S_{df} should be related to the laminar burning velocity S_L, which contains information about the speed of the chemical reaction. Departures from S_L reflect the mixture nonuniformities encountered during the propagation from f_{MR} to f_{st}, effects due to the pressure rise associated with autoignition, and effects of turbulence.

Values of S_{df} from simulations with different values of T_{ox}, T_{fu}, turbulence intensity, and initial δ so as to alter the autoignition time and the scalar dissipation rate at ignition, are

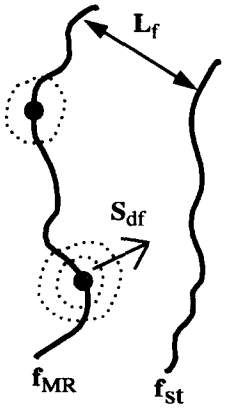

Fig. 15. Schematic of ignition front propagation from f_{MR} to f_{st}. S_{df} is the velocity at which the premixed gas is being consumed and is used to estimate the time lag between autoignition at f_{MR} and the establishment of the diffusion flame at f_{st}.

shown in Table 2. The velocity S_L is measured by separate runs of the code for a stoichiometric mixture at a temperature $T_{ox} - f_{st}(T_{ox} - T_{fu})$; the initial temperature is at f_{st}. Considering the large differences in f_{MR}, τ_{ign}, τ_{turb}, and Δt_{df} in the simulations, the observation that S_{df}/S_L is close to 0.5 for all simulations is very encouraging and suggests that the effect of the turbulence on Δt_{df} is captured by Eq. 10. With the approximation then that $S_{df}/S_L = 0.5$ and knowledge of the conditional scalar dissipation rate and of S_L, a time scale for the diffusion flame establishment after autoignition may be estimated.

3.4. Autoignition in Fuel Streams of Finite Extent

We examined in the Section 3.2 the first appearance of autoignition in infinite mixing layers and found that the ignition sites are located in regions with the most reactive mixture fraction and with low values of the conditional scalar dissipation rate $\chi|f_{MR}$. It was also shown that large initial δ and partial premixing ($f_o < 1$), and hence low $\chi|f_{MR}$, decrease the autoignition time. One additional way in which $\chi|f_{MR}$ may vary is by altering the initial length scale of the fuel stream and this mechanism is explored in this section.

We consider flows as depicted in Fig. 1b, with a slab of fuel surrounded by air at a high temperature. Two such simulations with identical initial interface thicknesses, partial premixing, and air temperature, but different slab widths, are compared. For the simulation with $w = 0.025$, $\tau_{ign} = 12.087$ while for $w = 0.050$, τ_{ign} is significantly longer at 13.754. Contours of the mixture fraction are shown in Figs. 16 and 17 for both cases just before ignition. It is evident that the f_{MR} contour (0.12) in the narrower flow has broken up due to mixing, and hence there exist spots that experience lower dissipation rates; hence the shorter autoignition times of the flow with small values of w.

In the limit of w becoming large compared to the turbulence scale, the flow on each side of the slab approaches that for an infinite layer. We expect then that the autoignition time increases with w to its value for the infinite layer. For the same initial turbulence time scale and δ, Table 3 shows autoignition times that increase from the flow with $w = 0.025$ to $w = 0.050$, with the highest value at the layer simulation. This trend is due to the increasing values of the scalar dissipation rate with flow width, as shown in greater detail below.

The volume-averaged value of the conditional dissipation $\langle \chi|f_{MR} \rangle$ was calculated from snapshots of the flow at many times until ignition, and the time evolution of $\langle \chi|f_{MR} \rangle$ is presented in Fig. 18 for layers and Fig. 19 for slabs. It is evident from all simulations that short autoignition times are associated with low values of $\langle \chi|f_{MR} \rangle$ and that, in general, slab flows autoignite earlier than infinite layers. Even if the initial value of $\langle \chi|f_{MR} \rangle$ were high due to thinner initial δ, because other parameters may have acted in such a way as to reduce $\langle \chi|f_{MR} \rangle$, the autoignition time may be reduced. For example, in Fig. 19, curve 4 initially has a higher scalar dissipation rate than curve 2, but, due to the smaller width of the flow, mixing of the f_{MR} contour is accomplished earlier. The conditional scalar dissipation decays faster and the autoignition time is hence shorter.

TABLE 2

Mean Velocity of the Ignition Front from Different Simulations[a]

T_{ox} (K)	T_{fu} (K)	f_{MR}	f_{st}	S_L/c_{ref}	τ_{turb}	τ_{ign}	Δt_{df}	S_{df}/c_{ref}	S_{df}/S_L
1100	300	0.12	0.055	0.0251	7.20	5.630	0.2770	0.0119	0.475
1000	300	0.12	0.055	0.0204	7.20	17.64	0.7230	0.0096	0.469
1000	300	0.12	0.055	0.0204	25.3	16.33	0.8340	0.0079	0.386
900	900	0.50	0.055	0.0177	7.20	7.350	1.5420	0.0109	0.616

[a] S_{df} is calculated from Eq. 10 and S_L is the laminar burning velocity of a stoichiometric mixture and unburnt temperature $T_{ox} - f_{st}(T_{ox} - T_{fu})$.

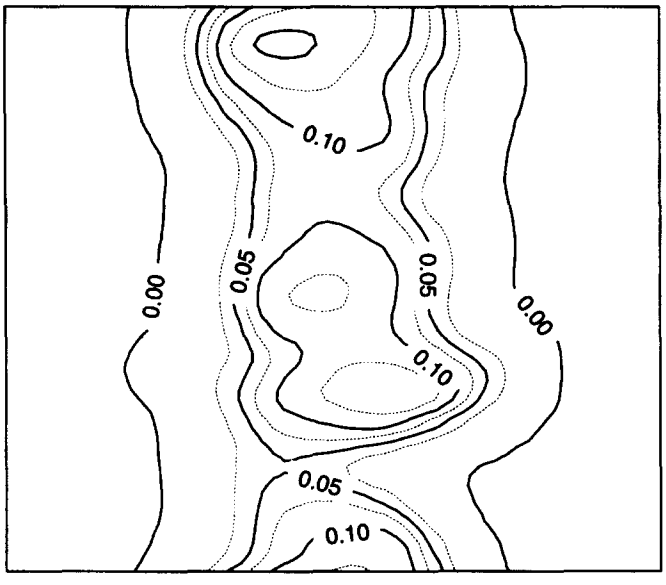

Fig. 16. Mixture fraction contours just before ignition for the slab flow of Table 3 with $w = 0.025$. Note the fragmented f_{MR} contour (0.12), which implies small gradients and thus low $\chi|f_{MR}$.

It is concluded from Sections 3.2 and 3.4 that all flow parameters such as flow width, turbulent length scales, turbulent time scales, and partial premixing, affect autoignition through their action on the conditional scalar dissipation rate.

3.5. Discussion

3.5.1. The Most Reactive Mixture Fraction

Liñan and Crespo [16] have analysed the ignition of a laminar one-dimensional mixing layer between cold fuel and warmer oxidant with high activation energy asymptotics and found that the temperature difference between the two streams and the activation energy determine *uniquely* the mixture fraction that will ignite. Here, we have confirmed this result for turbulent flows. For a qualitative understanding of the existence of a "preferred' mixture fraction for ignition, consider the expression for the reaction rate W:

$$W = Y_1 Y_2 \exp(-T_{act}/T), \tag{11}$$

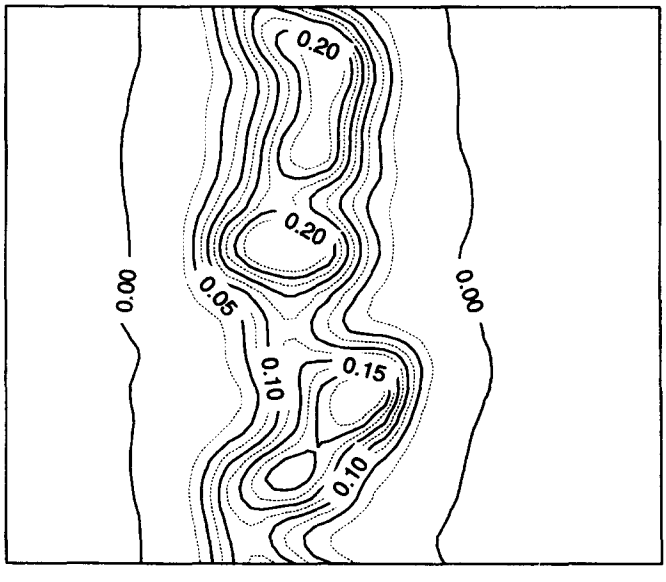

Fig. 17. Mixture fraction contours just before ignition for the slab flow of Table 3 with $w = 0.050$.

TABLE 3

Comparison of Autoignition Times in Slabs and Infinite Layers[a]

w	τ_{ign}/τ_{ref}
0.025	1.919
0.050	2.180
Layer	2.280

[a]For all simulations, $f_o = 0.5$, $\delta = 0.005$, $\tau_{turb} = 7.20$, $L_{turb} = 0.070$, $Re_t = 69$, and $T_{ox} = 1000$ K to give $\tau_{ref} = 6.309$.

which implies that the reaction rate is proportional to

$$f(1-f)\exp\left[\frac{-T_{act}}{T_{ox} - f(T_{ox} - T_{fu})}\right], \qquad (12)$$

assuming negligible temperature rise and consumption of reactants. The first two terms in Eq. 12 have a maximum at $f = 0.5$, but if $T_{ox} \neq T_{fu}$, the exponential dependence on the temperature in the third term moves the peak of the reaction rate toward lean (and hot) mixtures. Expression 12 therefore shows that the reaction rate will have a maximum at a well-defined mixture fraction which then determines the ignition location. This mixture fraction depends only on the order of reaction, the activation energy, and the temperatures of the two streams, and is close, but not identical, to the mixture fraction giving fastest ignition of the *homogeneous* mixtures of Fig. 2.

For the conditions of the present simulations, f_{MR} is found from plots like those in Fig. 9 for times before ignition for $T_{ox} = 1000$ and 1100 K to be around 0.12. In situations where the fuel and the oxidant temperatures are equal, as in one of the cases in Table 2, $f_{MR} = 0.5$. A detail concerning f_{MR}, evident in Fig. 9, is that the mixture fraction corresponding to the peak is shifted to slightly richer mixture fractions as time evolves, but most of this shift occurs very shortly before autoignition when the temperature increases much faster. For most of the time until ignition, the

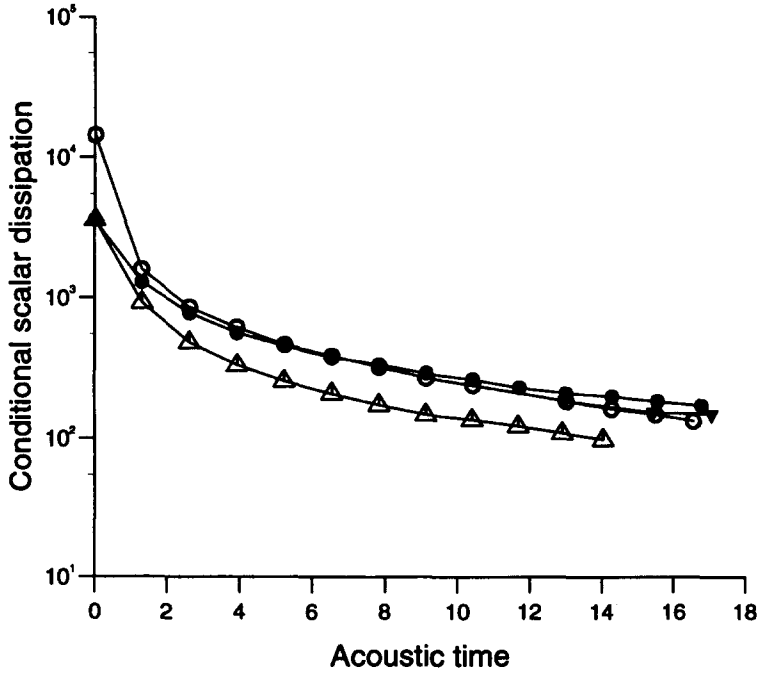

Fig. 18. Time evolution of conditionally averaged scalar dissipation rate $\langle \chi | f_{MR} \rangle$ until autoignition from the infinite layer simulations for $T_{ox} = 1000$ K giving $\tau_{ref} = 6.309$. Conditions are as follows: ●, $\tau_{turb} = 7.20$, $\delta = 0.010$, $f_o = 1.0$, $\tau_{ign} = 17.117$; ○, $\tau_{turb} = 7.20$, $\delta = 0.005$, $f_o = 1.0$, $\tau_{ign} = 16.394$; ▼, $\tau_{turb} = 10.56$, $\delta = 0.010$, $f_o = 1.0$, $\tau_{ign} = 15.883$; △, $\tau_{turb} = 4.22$, $\delta = 0.005$, $f_o = 0.5$, $\tau_{ign} = 14.065$.

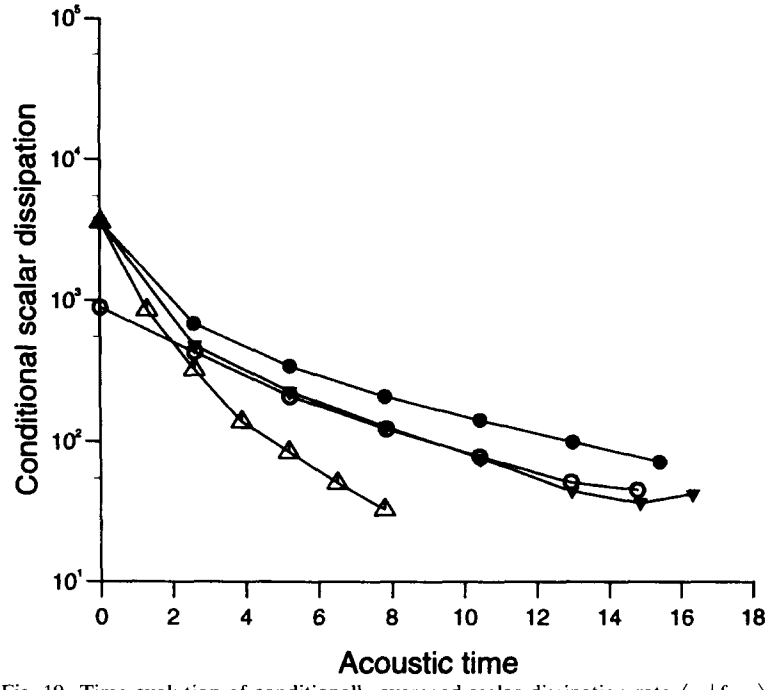

Fig. 19. Time evolution of conditionally averaged scalar dissipation rate $\langle \chi | f_{MR} \rangle$ until autoignition from slab simulations for $T_{ox} = 1000$ K giving $\tau_{ref} = 6.309$. Conditions are as follows: ●, $\tau_{turb} = 10.56$, $w = 0.030$, $\delta = 0.010$, $f_o = 1.0$, $\tau_{ign} = 15.520$; ○, $\tau_{turb} = 10.56$, $w = 0.050$, $\delta = 0.010$, $f_o = 0.5$, $\tau_{ign} = 14.000$; ▼, $\tau_{turb} = 7.20$, $w = 0.050$, $\delta = 0.005$, $f_o = 0.5$, $\tau_{ign} = 13.754$; △, $\tau_{turb} = 4.22$, $w = 0.025$, $\delta = 0.005$, $f_o = 0.5$, $\tau_{ign} = 12.087$.

peak is between 0.10 and 0.15 for the conditions of our simulations. This shift is due to the diffusion of heat produced at f_{MR} to richer mixtures which thus become the most reactive. When the temperature increment before ignition is small, as occurs in high activation energy reactions, this "shift" is negligible and will not be considered further.[2] The value of f_{MR} is very accurately predicted in Ref. 16 (Fig. 7) and that work should be consulted for numerical values for high activation energy reactions. As an example of the application of their results, consider *n*-heptane autoignition under diesel engine conditions: we estimate that $f_{MR} = 0.07$ for $T_{fu} = 500$ K, $T_{ox} = 1000$ K, and an activation energy of 18,367 K [18].

There is evidence that complex chemistry effects may alter this picture for heavy hydrocarbons that have a nonmonotonic dependence of autoignition time on temperature [19]. Such a dependence suggests that autoignition is not just a "thermal runaway" phenomenon and that the temperature is not the only determining factor in ignition. The competition between hydrogen abstraction and fuel breakdown reactions that are favoured at different temperatures makes autoignition less sensitive to temperature than the one-step Arrhenius description implies. This then suggests that f_{MR} cannot be determined from the analysis of Ref. 16 and that the dependence on the scalar dissipation rate, which affects the heat losses, may be less pronounced. Simulations with complex chemistry would be helpful to clarify these issues.

[2] The same argument explains why f_{MR} and the mixture fraction found from Eq. 12 and corresponding to τ_{ref} in Fig. 2 are not exactly equal. Both Eq. 12 and the homogeneous mixture calculations of Fig. 2 do not consider heat diffusion across mixture fraction space. In the inhomogeneous flows, however, heat released during the induction time before autoignition is diffused toward richer mixture fractions which accelerate the reaction there, making it the fastest. This effect is included in the calculation of f_{MR} in Ref. 16.

3.5.2. The Effect of Turbulence on Autoignition

A conclusion of this work is that, in the flows examined, τ_{ign}/τ_{ref} was in the range 1.8–2.8. The minimum possible autoignition time of initially separate fuel–air of given temperatures is τ_{ref} and would be observed in infinitely fast mixing of adiabatic flows, as discussed in Section 3.1. Therefore mixture inhomogeneities delay ignition. Since this delay is attributed here to the heat losses necessarily accompanying mixture fraction gradients during the induction time, fast turbulence or small flow scales, by destroying these gradients quickly and creating well-mixed spots, may *facilitate* autoignition. This is to be contrasted to the trend expected by extrapolating to turbulent mixing flows the results of strained laminar autoigniting layers [7–9], where the effect of strain, which is high in fast turbulence, is to increase the delay time.

This discrepancy is easily understood by realising that the proper parameter to describe the laminar-like mixing layers in turbulent flows is the local scalar dissipation rate, not the strain rate [20], and that χ does not depend only on τ_{turb}. Indeed, Fig. 12 shows that there is no large effect of τ_{turb} on τ_{ign}, at least in the range $\tau_{ign} < \tau_{turb}$, but Figs. 18 and 19 show a dependence on χ. Consider also Fig. 17: the initial size of the fuel stream determines the size of the f_{MR} regions, which then determine $\chi|f_{MR}$ and the heat losses. Even if the two flows in Fig. 17 experience the same straining, the heat losses are different due to the different size of the f_{MR} spots, resulting in different ignition times. Finally, Fig. 19 shows that for flows with fast turbulence or small scale, even if the initial value was high, χ decays quickly and so may remain low for a long period before ignition, and hence τ_{ign} is shortened.

Therefore the effects of the turbulence on autoignition time can be better understood by proper consideration of the relationship between τ_{turb} and $\chi|f_{MR}$. Although usually these two quantities are inversely proportional, χ has been shown to depend additionally on the scalar length scale and on the time relative to τ_{turb} [21, 22]. In Monte Carlo simulations of autoignition [23–25] of flows with a constant and uniform mean value of the mixture fraction, but with large fluctuations implying finite scalar dissipation, the autoignition time was reduced with decreasing τ_{turb} in the range $\tau_{ign} \gg \tau_{turb}$. The present results are not inconsistent and provide the explanation that a fast turbulence causes fast mixing, well-mixed spots with low $\chi|f_{MR}$ are created, and hence autoignition is favoured.

3.5.3. Implications for Spray Autoignition

An implication of our conclusion that τ_{ign}/τ_{ref} is greater than unity and flow dependent is that ignition times observed in spray experiments cannot be exactly similar to those measured in shock tubes because, in the former, mixture inhomogeneities increase the delay. Although we do not expect this to affect inferred quantities like the overall activation energy [6], it possibly affects the ignition times measured in Ref. 4. Indeed, these authors made a comparison between their autoignition data with those in shock tubes and found that the former are longer, in agreement with our finding that τ_{ign}/τ_{ref} is larger than 1.

An additional conclusion of this work is that the randomness observed in the first appearance of autoignition in individual realisations of the same flow is small. This is to be contrasted to recent measurements in sprays [1, 26] that showed autoignition times with r.m.s. fluctuations divided by the mean on the order of 20%. We thus conjecture that the observed randomness was due to fluctuations of $\chi|f_{MR}$ introduced by fuel concentration fluctuations created during atomisation and evaporation, rather than by the turbulence. Experimental data on *gaseous* autoigniting flows are necessary to clarify this point.

Finally, we note that mixing of fuel slabs (as in Fig. 16) rather than infinite layers may be relevant to the way fuel mixes with air before ignition in jet engine afterburners, where autoignition is desired, and in premixed gas turbines, where fast mixing is required before the combustor and autoignition should be avoided at all costs. The present results may help in identifying operational regimes of practical configurations since, by comparisons with the ignition times of homogeneous mixtures, we have quantified the delay introduced by the turbulence. Similarly, we may conjecture that

multihole diesel sprays ignite earlier than single-hole sprays (as Table 3 shows) due to the smaller conditional scalar dissipation rates expected after the faster breakup and mixing of the narrower fuel streams.

3.5.4. Implications for Modelling

The conclusion that the autoignition sites are those of low $\chi|f_{MR}$ and with composition given by f_{MR} has profound implications for the way modelling of autoignition should be attempted. For example, in Monte Carlo calculations such as those in Refs. 23–25, special attention should be given to the accurate calculation of the conditional scalar dissipation rate. The standard "interaction with the mean" models for the molecular diffusion terms [27] that represent the heat loss during the induction time use a mixing time scale independent of mixture fraction and may hence be inadequate.

Similarly, in moment closures with flamelet models [19], proper account should be taken of the conditional $\chi|f_{MR}$, rather than of an unconditional average value. Due emphasis on the conditionally averaged quantities is given in the conditional moment closure of Bilger [28], where models for $\langle \chi|f_{MR} \rangle$ are examined and compared with the conventional average scalar dissipation rate at the spatial location where the mean mixture fraction has its most reactive value. A standard moment closure can calculate the latter but not the former. Indeed, in flows where the mean mixture fraction decays due to mixing to a value less than f_{MR}, which is what may happen in a mixing flow of finite width and cannot happen in a flow with sustained extreme values, the unconditional scalar dissipation rate becomes a quantity that cannot be calculated at all. Autoignition, however, will still happen in fluid with $f = f_{MR}$ because the reaction rate always peaks there, and this suggests that proper modelling approaches for autoignition should be based on conditional quantities, rather than unconditional ones.

4. CONCLUSIONS

Two-dimensional direct numerical simulations have been performed of the autoignition in turbulent shearless mixing layers to clarify the influence of turbulence on the time and location of the first ignition site, motivated in part by recent experimental evidence of igniting diesel sprays that show large and unexplained scatter in ignition times and locations. The flows considered were (i) a mixing layer between fuel and air at elevated temperatures, (ii) a slab of width w of fuel in air, both flows with an initially isotropic and homogeneous but decaying turbulent field of initial time scale τ_{turb} and length scale L_{turb}, and (iii) homogeneous, stagnant adiabatic mixtures for comparison purposes.

Chemical reaction rates were described by a one-step Arrhenius law of high activation energy and the heat release and stoichiometry of methane. The initial mass fractions of fuel and oxygen and the initial temperature were determined as in inert mixing by the prescribed error-function profile of the mixture fraction f, with characteristic thickness δ to give values of zero and f_o in the air and fuel streams, respectively. Values of f_o smaller than unity allow for partial premixing, as may occur, for example, in fuel streams created by liquid droplet evaporation.

When the initial temperature and reactant concentrations of a homogeneous autoigniting fluid were not independent, but related as in inert mixing of initially separate fuel and air of different temperatures and thus fully characterised by the mixture fraction, the autoignition time showed a minimum τ_{ref} at a mixture fraction around 0.11 for the chosen values of T_{fu}, T_{ox}, and T_{act}. This was due to the beneficial effect on the reaction rate of the high initial temperatures at very lean mixtures balancing the detrimental effect of reduced fuel concentration, resulting thus in an optimum mixture fraction with the highest reaction rate and shortest ignition time.

Results from calculations in turbulent flows led to the following conclusions for the autoignition time:

(i) the variation of τ_{ign} observed in individual realisations of the same flow was about 5% for $\tau_{ign} < \tau_{turb}$ and about 10% for $\tau_{ign} > \tau_{turb}$;

(ii) τ_{ign} was, surprisingly, independent of τ_{turb} for given initial f_o, δ, and w;

(iii) τ_{ign}/τ_{ref} varied between 1.8 and 2.8, with low values associated with small w, and thus
(iv) flows with finite extent of the fuel stream (slabs) ignited earlier than infinite layers ($w \to \infty$);
(v) τ_{ign} decreased with increasing initial δ;
(vi) partial premixing reduced τ_{ign}, and
(vii) turbulent flows ignite earlier than laminar ones.

Examination of two-dimensional contours and scatter plots showed that the first occurrence of ignition was always at mixture fractions very close to the most reactive mixture fraction, f_{MR}, determined in the analysis of Liñan and Crespo [16] for laminar autoigniting mixing layers to depend only on the initial fuel and oxidant temperatures and the activation energy. The value of f_{MR} was also close to the mixture fraction that gives the fastest ignition of the adiabatic homogeneous mixtures.

The time taken for combustion to reach the stoichiometric mixture fraction following ignition at f_{MR} was also calculated from the simulations. It was found that the mean velocity at which the ignition fronts propagate to span the physical space between f_{MR} and f_{st} was about 0.5 of the laminar burning velocity of a stoichiometric mixture. Thus, with knowledge of the distance between the ignition and stoichiometric mixture fractions, which depends on the mixing field, the time needed for the complete ignition of the diffusion flame after autoignition can be estimated.

The second characteristic of ignition was that it always occurred at sites along the f_{MR} contour that had the lowest values of the dissipation rate of the mixture fraction χ. This finding was confirmed by calculations of the correlation coefficient between the local reaction rate and the scalar dissipation rate conditional on the mixture fraction which showed large negative values in the proximity of f_{MR} until autoignition. It was thus concluded that high values of the reaction rate are associated with low values of the conditional scalar dissipation rate $\chi|f_{MR}$, and examination of the time evolution of the volume average $\langle \chi|f_{MR} \rangle$ until autoignition from numerous calculations showed that small values of τ_{ign} occurred always when $\langle \chi|f_{MR} \rangle$ was low.

This result, understood qualitatively by considering that if $\chi|f_{MR}$ were high, the heat losses from the most reactive heat-producing regions in the flow are high, explains all the trends found for τ_{ign} with δ, w, f_o, and τ_{turb}. In particular, the low randomness of τ_{ign} is understood because in any realisation, regions of low $\chi|f_{MR}$ will always be present and it is these regions that will first ignite. This then suggests that the large scatter in the autoignition time observed in spray experiments is due to random aspects of atomisation and evaporation, rather than due to the turbulence in the gaseous phase, but also that the spatial scatter of ignition sites is due to the random spatial distribution of regions with $f = f_{MR}$ and low χ. The present results suggest that chemical data inferred from spray ignition studies cannot be fully equivalent to those in shock tubes because mixture inhomogeneities imply heat losses, and these may increase the autoignition time by a factor of about 2–3. Finally, the dependence of τ_{ign} on $\chi|f_{MR}$, rather than simply τ_{turb}, requires that modelling efforts of autoignition in turbulent inhomogeneous mixing flows should concentrate on the accurate modelling of the conditional scalar dissipation rate.

This work was performed in the Centre de Recherche sur la Combustion Turbulente in IFP, whose financial assistance is acknowledged. Thanks are due Dr. Benedicte Cuenot and Dr. Markus Baum of CERFACS, E. van Kalmthout of Ecole Centrale de Paris, Dr. Arnaud Trouve of IFP, and Dr. Tarek Echekki of CRCT-IFP, now at Sandia National Laboratories, for useful discussions.

REFERENCES

1. Baritaud, T. A., Heinze, T. A., and Le Coz, J.-F., *Spray and Self-Ignition Visualisation in a DI Diesel Engine*, SAE Paper No. 940681, 1994.
2. Sato, J., Konishi, K., Okada, H., and Niioka, T., *Twenty-First Symposium (International) on Combustion*, The Combustion Institute, Pittsburgh, 1986, p. 695.

3. Neraud, E., *Modelisation Diesel. Modelisation de l'Auto-Inflammation et de la Combustion Diesel. Evaluation et Ajustement de Modeles Physiques*, IFP Internal Report No. 41274, 1994.
4. Cavaliere, A., Ciajolo, A., D'Anna, A., Mercogliano, R., and Ragucci, R., *Combust. Flame* 93:279 (1993).
5. Ciezki, H. K., and Adomeit, G., *Combust. Flame* 93:421 (1993).
6. Mizutani, Y., Nakabe, K., and Chung, J. D., *Twenty-Third Symposium (International) on Combustion*, The Combustion Institute, Pittsburgh, 1990, p. 1455.
7. Thevenin, D., and Candel, S., *Combust. Sci. Technol.* 91:73 (1993).
8. Liñan, A., and Williams, F. A., *Combust. Flame* 95:31 (1993).
9. Liñan, A., *Acta Astronautica* 1:1007 (1974).
10. Poinsot, T., Veynante, D., and Candel, S., *J. Fluid Mech.* 228:561 (1991).
11. Cuenot, B., and Poinsot, T., *Twenty-Fifth Symposium (International) on Combustion*, The Combustion Institute, Pittsburgh, 1994, p. 1383.
12. Westbrook, C. K., and Dryer, F. L., *Combust. Sci. Technol.* 27:31 (1981).
13. Cuenot, B., and Poinsot, T., *Combust. Flame* 104:111 (1996).
14. Baum, M., and Poinsot, T., *A Direct Simulation Code for Studies of Combustion Phenomena*, Internal Report, EM2C/CNRS, Ecole Centrale de Paris, 1993.
15. Poinsot, T., and Lele, S., *J. Comput. Phys.* 101:104.
16. Liñan, A., and Crespo, A., *Combust. Sci. Technol.* 14:95.
17. Corcione, F. E., and Fusco, A., *Fourth International KIVA Users Meeting*, Detroit, February 27, 1994.
18. Li, S. C., Libby, P. A., and Williams, F. A., *Twenty-Fourth Symposium (International) on Combustion*, The Combustion Institute, Pittsburgh, 1992, p. 1503.
19. Muller, U. C., Pitsch, H., Wan, Y. P., and Peters, N., *EUROMECH Colloquium 324*, Marseille, July 25–27, 1994.
20. Peters, N., *Twenty-First Symposium (International) on Combustion*, The Combustion Institute, Pittsburgh, 1986, p. 353.
21. Eswaran, V., and Pope, S. B., *Phys. Fluids* 31:506 (1988).
22. Warhaft, Z., and Lumley, J. L., *J. Fluid Mech.* 88:659 (1978).
23. Bruel, P., Rogg, B., and Bray, K. N. C., *Twenty-Third Symposium (International) on Combustion*, The Combustion Institute, Pittsburgh, 1990, p. 759.
24. Lakshmisha, K. N., Zhang, Y., Rogg, B., and Bray, K. N. C., *Twenty-Fourth Symposium (International) on Combustion*, The Combustion Institute, Pittsburgh, 1992, p. 421.
25. Correa, S. M., and Dean, A. J., *Twenty-Fifth Symposium (International) on Combustion*, The Combustion Institute, Pittsburgh, 1994, p. 1293.
26. Cavaliere, A., Unpublished work, University of Napoli, 1992.
27. Borghi, R., *Prog. Energy Combust. Sci.* 14:245 (1988).
28. Bilger, R. W., *Phys. Fluids A* 5:437 (1993).

Received 6 February 1995